

Measurement of dipole matrix elements with a single trapped ion

M. Hettrich,^{1,*} T. Ruster,¹ H. Kaufmann,¹ C. F. Roos,^{2,3} C. T. Schmiegelow,¹ F. Schmidt-Kaler,¹ and U. G. Poschinger¹

¹QUANTUM, Institut für Physik, Universität Mainz, Staudingerweg 7, 55128 Mainz, Germany[†]

²Institut für Quantenoptik und Quanteninformation, Österreichische Akademie der Wissenschaften, Technikerstraße 21a, 6020 Innsbruck, Austria

³Institut für Experimentalphysik, Universität Innsbruck, Technikerstraße 25, 6020 Innsbruck, Austria

(Dated: April 25, 2022)

We demonstrate a new method for the direct measurement of atomic dipole transition matrix elements based on techniques developed for quantum information purposes. The scheme consists of measuring dispersive and absorptive off-resonant light-ion interactions and is applicable to many atomic species. We determine the dipole matrix element pertaining to the Ca II H line, i.e. the $4^2S_{1/2} \leftrightarrow 4^2P_{1/2}$ transition of $^{40}\text{Ca}^+$, for which we find the value $2.893(8) \text{ ea}_0$. Moreover, the method allows us to deduce the lifetime of the $4^2P_{1/2}$ state to be $6.90(5) \text{ ns}$, which is in agreement with predictions from recent theoretical calculations and resolves a longstanding discrepancy between calculated values and experimental results.

PACS numbers: 37.10.Ty, 37.10.-x, 32.80.Qk, 03.67.Lx

Methods for trapping and cooling single or few atoms, molecules or ions and manipulating them at the quantum level have opened up new avenues for precision laser spectroscopy. In particular, quantum logic techniques [1] have enabled a new accuracy regime of timekeeping with optical atomic clocks [2]. In contrast to atomic transition frequencies, dipole matrix elements and radiative lifetimes are still notoriously hard to measure at high precision. The accurate and precise determination of these quantities is of importance for the quantification of black body radiation shifts of atomic clocks [3], interpretation of astrophysical spectra [4, 5], novel approaches for the search for physics beyond standard model [6, 7] and for testing the accuracy of atomic structure calculations [8]. For the measurement of radiative lifetimes and transition matrix elements, established methods e.g. based on ion beams have been successfully complemented by novel techniques based on trapped particles. For ^{87}Rb , dipole matrix elements have been determined on the 10^{-3} accuracy level by diffraction in a condensate [9], while for the $6p^2P_{1/2}^O$ state of $^{174}\text{Yb}^+$, the radiative lifetime has been measured by time-resolved counting of photons emitted from a single trapped ion [10]. A related technique was used for neutral ^{171}Yb in an optical lattice [11]. The species Ca^+ is widely used in quantum optics experiments, and its II H line led to the discovery of the interstellar medium [12]. For $^{40}\text{Ca}^+$, branching ratios between different decay channels have been determined at accuracies approaching the 10^{-5} level [13, 14], and lifetimes of metastable states have been accurately measured [15]. The $4^2P_{1/2}$ radiative lifetime has been determined to be $7.098(20) \text{ ns}$ [16] by fluorescence measurements on a fast ion beam. However, this value deviates by more than 11 standard deviations from the most recent theoretical calculation [8], while similar calculations for alkaline-like species from Li to Fr, Mg^+ , Ba^+ and Sr^+ are in good

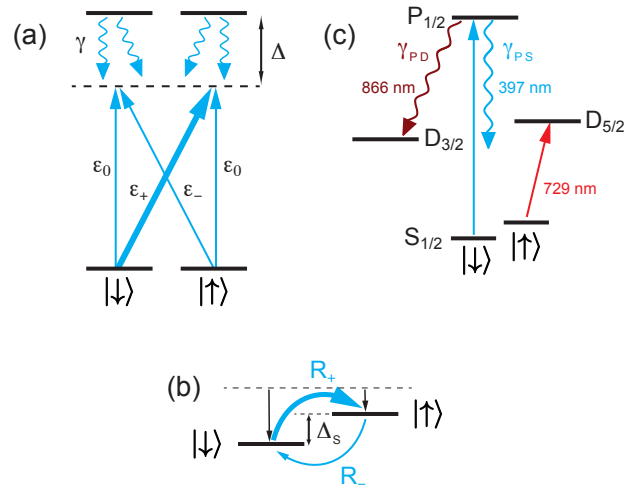


FIG. 1. (color online) Measurement scheme: (a) a laser off-resonantly couples two Zeeman ground state levels to an excited state with decay rate γ . (b) The coupling gives rise to a differential ac-Stark shift Δ_S between the Zeeman levels and incoherent redistribution of population at rates R_{\pm} . (c) Relevant energy levels in $^{40}\text{Ca}^+$. The shelving to the metastable $3^2D_{5/2}$ state as well the $3^2D_{3/2}$ state acting as a population sink are indicated.

agreement with experimental results (see [8] and references therein). In this work, we present a measurement of the radiative decay rates of the $4^2P_{1/2}$ excited state of $^{40}\text{Ca}^+$. It is based on techniques used for preparation, coherent manipulation and read-out of atomic states developed for ion trap quantum computing [17, 18]. As our scheme works with a single trapped ion and discrete discrimination of atomic states rather than temporal or spatial quantification of resonance fluorescence counts, it is robust against many systematic error sources which affect other existing methods. Our method allows for the determination of one specific matrix element even in the

presence of other decay channels, and it is applicable to atom and ion species which allow for preparation and readout of Zeeman or hyperfine sublevels.

The cornerstone of the method is the comparison between *dispersive* and *absorptive* interaction of a single $^{40}\text{Ca}^+$ ion with an off-resonant laser beam, which provides dipolar coupling of the $4^2\text{S}_{1/2}$ ground state to the $4^2\text{P}_{1/2}$ excited state. The laser electric field at the position of the ion is $\mathbf{E}(t) = \sum_{q=\pm,1} \mathcal{E}\epsilon_q \mathbf{e}_q e^{-i\omega_0 t} + c.c.$, where the ϵ_q characterize the relative amplitudes of the circular ($q = \pm 1$, denoted '±' henceforth) and π ($q = 0$) polarization components, ω_0 is the optical frequency, \mathbf{e}_q are the spherical basis vectors and \mathcal{E} is the electric field amplitude. The coupling is described by the Rabi frequency $\Omega = 2\mathcal{E}\mathcal{D}/\hbar$, where $\mathcal{D} = \langle S_{1/2} || \hat{\mathbf{d}} || P_{1/2} \rangle$ is the reduced matrix element of the dipole operator. The polarization components ϵ_q drive transitions between Zeeman sublevels with $m_P - m_S = q$ at effective Rabi frequencies scaled with the respective Wigner 3j-symbol, $\Omega\epsilon_q \begin{pmatrix} 1/2 & 1 & 1/2 \\ -m_S & q & m_P \end{pmatrix}$. The radiative decay rate from the $P_{1/2}$ to the $S_{1/2}$ state, γ_{PS} , is related to \mathcal{D} by

$$\mathcal{D}^2 = 2\gamma_{PS} \frac{3\epsilon_0 \hbar}{8\pi^2} \lambda_{PS}^3, \quad (1)$$

where λ_{PS} is the resonance wavelength. The laser is detuned far from the power-broadened resonance, by a frequency $|\Delta| \gg \Omega, \gamma_{PS}$.

The *dispersive* interaction with the laser causes ac Stark shifts of the energy levels, which is exploited in atomic physics e.g. for optical trapping [19] of atoms or for quantum state manipulation of trapped ions [20, 21]. In our scheme, we are interested in the differential ac Stark shift Δ_S between the two Zeeman-sublevels of the electronic ground state $|S_{1/2}, m_S = \pm 1/2\rangle$, denoted henceforth as $|\uparrow\rangle$ and $|\downarrow\rangle$:

$$\Delta_S = \frac{1}{3} \frac{\Omega^2}{4\Delta} (\epsilon_-^2 - \epsilon_+^2), \quad (2)$$

The *absorptive* interaction manifests itself through inelastic Raman scattering, i.e. spin flips [22, 23]. R_+ denotes the spin flip rate from $|\downarrow\rangle$ to $|\uparrow\rangle$ and R_- the rate in the inverse direction respectively. For a beam with arbitrary polarization this reads [20]

$$R_{\pm} = \gamma_{PS} \frac{\epsilon_{\pm}^2 + \epsilon_0^2}{9} \frac{\Omega^2}{4\Delta^2} \quad (3)$$

Note that the π -polarized light drives the two spin-flip directions equally strong, whereas each of the the circular components drives only one pathway, corresponding to optical pumping in the limit of purely circularly polarized light. The occurrence of elastic (Rayleigh) scattering is taken into account. For population leakage by decay to the $3^2\text{D}_{3/2}$ state at rate γ_{PD} , we make the assumption that only circular components are present in the beam, i.e. $\epsilon_0^2 \approx 0$, which is justified below. Then, one out of three photon scattering events leads to a spin flip. The

rates at which population from $|\uparrow\rangle$ ($|\downarrow\rangle$) is sunk in the metastable $3^2\text{D}_{3/2}$ state are then given by

$$R_{\uparrow(\downarrow)D} = 3(\gamma_{PD}/\gamma_{PS})R_{-(+)}. \quad (4)$$

The spin-flip dynamics can then be described by the rate equations:

$$\begin{aligned} \dot{p}_{\uparrow} &= -R_-(1+b)p_{\uparrow} + R_+p_{\downarrow} \\ \dot{p}_{\downarrow} &= -R_+(1+b)p_{\downarrow} + R_-p_{\uparrow}. \end{aligned} \quad (5)$$

with the leak factor $b = 3(\gamma_{PD}/\gamma_{PS})$. The solution of Eqs. 5 is

$$\begin{aligned} \dot{p}_{\uparrow}^{(\uparrow)}(t) &= \frac{1}{\bar{R}} e^{-\frac{1}{2}\bar{R}t} \left(\tilde{R} \cosh\left(\frac{\tilde{R}t}{2}\right) - (1+b)\delta R \sinh\left(\frac{\tilde{R}t}{2}\right) \right) \\ \dot{p}_{\uparrow}^{(\downarrow)}(t) &= \frac{2}{\bar{R}} e^{-\frac{1}{2}\bar{R}t} R_+ \sinh(\tilde{R}t/2), \end{aligned} \quad (6)$$

with $p_{\uparrow}^{(\uparrow)}$ corresponding to initialization in $|\uparrow\rangle$, $p_{\uparrow}(t=0) = 1$, and $p_{\uparrow}^{(\downarrow)}$ for initialization in $|\downarrow\rangle$, $p_{\uparrow}(t=0) = 1$. We use $\bar{R} = (1+b)(R_- + R_+)$ and $\tilde{R}^2 = \bar{R}^2 - 4b(2+b)R_-R_+$. Combining Eqs. 2 and 3, the decay rate γ_{PS} reads

$$\gamma_{PS} = 3\Delta \frac{\delta R}{\Delta_S}, \quad (7)$$

with $\delta R = R_- - R_+$. All quantities on the rhs of 7 are independently experimentally accessible, which allows us to determine γ_{PS} . The Rabi frequency Ω , which is hard to determine experimentally, does not appear in that expression.

We perform measurements on a single $^{40}\text{Ca}^+$ ion stored in a segmented Paul trap [24]. The relevant energy levels and transitions are depicted in Fig. 1. The Zeeman sublevels of the electronic ground state $|\uparrow\rangle$ and $|\downarrow\rangle$ are split by $2\pi \times 13.7$ MHz. We perform Doppler cooling on the $4^2\text{S}_{1/2} \leftrightarrow 4^2\text{P}_{1/2}$ (cycling) transition near 397 nm. After cooling, the ion is prepared in either $|\uparrow\rangle$ or $|\downarrow\rangle$ by optical pumping. After the state manipulations described below, spin read-out is accomplished by shelving population from the $|\uparrow\rangle$ level to the metastable $3^2\text{D}_{5/2}$ state by means of rapid adiabatic passage (RAP) pulses [18, 25]. The ion is then illuminated by laser fields driving the cycling transition and the $3^2\text{D}_{3/2} \leftrightarrow 4^2\text{P}_{1/2}$ transition near 866 nm, such that fluorescence is detected on a photomultiplier tube if the ion is not in the metastable $3^2\text{D}_{5/2}$ state. The probability of fluorescence detection therefore corresponds to the population being in the $|\downarrow\rangle$ and $3^2\text{D}_{3/2}$ states after the manipulation. The off-resonant light near 397 nm is provided by an amplified and frequency-doubled diode laser system, stabilized in both wavelength ($\delta\Delta/\Delta \lesssim 0.5 \cdot 10^{-3}$) and intensity ($\delta I/I \lesssim 0.5 \cdot 10^{-3}$). The beam is aligned along the quantizing magnetic field and predominantly σ^+ polarized, such that $R_+ \gg R_-$, and $\epsilon_0^2 \approx 0$, justifying the approximation for Eq. 4. The measurement of the ac Stark shift Δ_S is accomplished by performing a spin-echo technique: A $\pi/2$ pulse on the stimulated Raman transition between $|\uparrow\rangle$ and $|\downarrow\rangle$

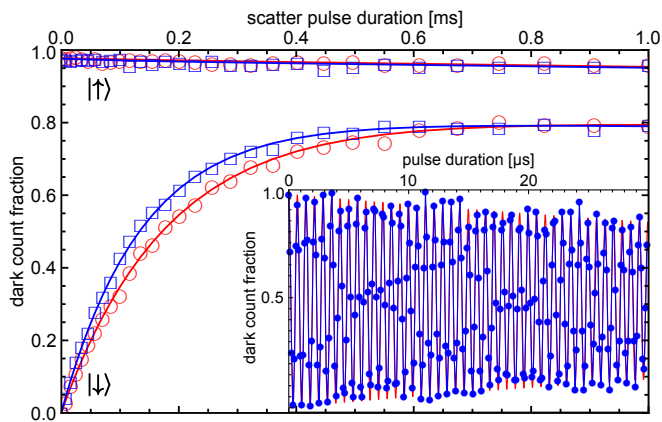


FIG. 2. (color online) Dark count fraction versus time of exposure to an off-resonant laser pulse for initializations in $|\uparrow\rangle$ and $|\downarrow\rangle$. Data points indicated by blue squares (red circles) are measured with the laser detuned by 12.03 GHz (13.94 GHz) from resonance. Solid lines show the fits to the model Eq. (6). The inset shows the dark count fraction versus pulse duration for a spin-echo experiment. The blue line connects the datapoints, the red line is the resulting fit. The oscillation frequency directly corresponds to the differential ac Stark shift Δ_S .

is followed by a π pulse, another $\pi/2$ pulse concludes the sequence. The delay time between the pulses is constant. During the first delay, the ion is exposed to an off-resonant square pulse of variable duration. We probe 250 different shift pulse times, each with 150 interrogations. The times are spaced by 120 ns, such that a signal with about 40 oscillation periods is obtained. The differential ac Stark shift is the frequency of this oscillatory dark count fraction (see inset of Fig. 2).

For the measurement of the spin-flip rates R_{\pm} , the ion is exposed to pulses of variable duration up to 1 ms of the off-resonant laser after preparation. In contrast to the ac Stark shift measurement, the required quantities are slopes rather than a frequency, thus substantially more data has to be acquired in order to reduce the impact of readout shot noise. For each measurement, the dark count fraction is determined by probing the ion 2500 times for 30 fixed scatter pulse durations. The resulting total dark count fractions versus pulse time are shown in Fig. 2. The time gap between initialization and readout is kept constant irrespectively of the scatter pulse duration to avoid systematic effects. We extract the parameters δR and b from the spin flip data by means of a Markov chain Monte Carlo parameter estimation, taking into account the binomial statistics of the quantum projection noise in the spin readout. State preparation and measurement errors are taken into account by modeling the measured dark count fractions as a linear transformation of the values $\dot{p}_{\uparrow}^{(\uparrow)}(t), p_{\uparrow}^{(\downarrow)}(t)$ from Eqs. 6.

65 independent data sets were taken, each comprised of spin flip rate measurements for preparation both in $|\uparrow\rangle$ and $|\downarrow\rangle$, and ac Stark shift measurements taken directly

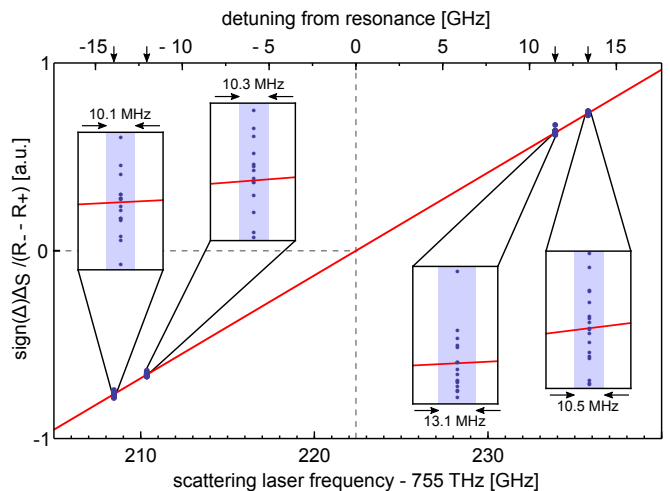


FIG. 3. (color online) Determination of the four detunings chosen for our measurements. For each of the 65 acquired datasets, we plot the quantity $\text{sign}(\Delta)\Delta_S/\delta R \propto \Delta$ versus the optical frequency as measured by a wavelength meter. The zero crossing of a linear fit, depicted by the solid red line, reveals the resonance frequency with a standard error of $2\pi \cdot 21$ MHz. The insets show details of the datasets measured at the different detunings with the abscissa magnified 166 times. The shaded backgrounds indicate their uncertainties along the frequency axis. The arrows on the top frequency scale indicate the values of the four different detunings at -13.94, -12.03, 11.52 and 13.42 GHz.

before and after the spin flip measurements in order to capture drifts of the laser intensity and thus the Rabi frequency Ω . The total data acquisition time was about 50 h. The acquired data sets are taken for four different laser detunings. To determine the value of these detunings, we read the optical frequency from a commercial wavelength meter (High Finesse WSU 267) with better than 10 MHz precision. We perform a linear regression of the measured Δ_S divided by δR versus the corresponding optical frequencies to obtain the resonance frequency, as shown in Fig. 3. Compared to direct fluorescence spectroscopy, this technique mitigates effects like power broadening, Zeeman splitting micro motion-induced broadening, which would make a determination of the resonance frequency less accurate.

We combine the measured quantities Δ, Δ_S and δR , using Eq. 7, to obtain the desired value γ_{PS} . Together with b this also yields $\gamma_{PD} = \frac{b}{3}\gamma_{PS}$. The radiative lifetime is given by $1/\tau = \gamma_{PS}(1 + \frac{b}{3})$. Averaging over the data sets and taking into account the corrections discussed below, we obtain the resulting values: $\gamma_{PS} = 2\pi \times 21.57(15)$ MHz and a $4^2P_{1/2} \rightarrow 4^2S_{1/2}$ branching fraction of $1/(1 + \frac{b}{3}) = 0.9357(4)$. This leads to a lifetime of $\tau = 6.90(5)$ ns and a value of $\gamma_{PD} = 2\pi \times 1.481(15)$ MHz. Together with the absolute wavelength λ_{PS} of the $4^2S_{1/2} \leftrightarrow 4^2P_{1/2}$ transition, we obtain the reduced matrix element \mathcal{D} of the respective transition as well, using Eq. 1. We determine a

value of $\mathcal{D} = 2.893(8) \text{ ea}_0$. Experimental imperfections and model approximations lead to errors and corrections for the value of γ_{PS} . These are summarized in Table I: Beyond the approximation in Eq. 4, a possible ϵ_0 polarization component has been taken into account, and yields corrections and systematic errors on the 10^{-3} level. The precision of the detuning Δ is limited by the wavelength meter, and its accuracy is limited by the determination of the resonance frequency. Statistical uncertainties of the measurement values δR and b , determined by the amount of acquired data, represent a major contribution to the error budget. Residual resonant light close to 397 nm resulting from imperfect laser switch-off causes relative corrections and systematic errors in the 10^{-4} regime. Beyond the rate equation model Eq. 5, we include a correction for the finite lifetime of the $3^2D_{3/2}$ state or its depletion by residual light near 866 nm. Δ_S can be measured by orders of magnitude more precisely than δR and b , however the precision is limited by drift effects, quantified by monitoring the ac Stark shift over the entire data acquisition time. Excess micromotion of the ion also causes a small systematic error via frequency modulation of the off-resonant light. Furthermore, we include corrections due to the presence of the $4^2P_{3/2}$ state about $2\pi \times 6.69$ THz above the $4^2P_{1/2}$ state, and due to the power-broadened Lorentzian lineshape beyond the assumption $|\Delta| \gg \Omega, \gamma_{PS}$. A detailed discussion of corrections and errors is presented in the supplemental material [?].

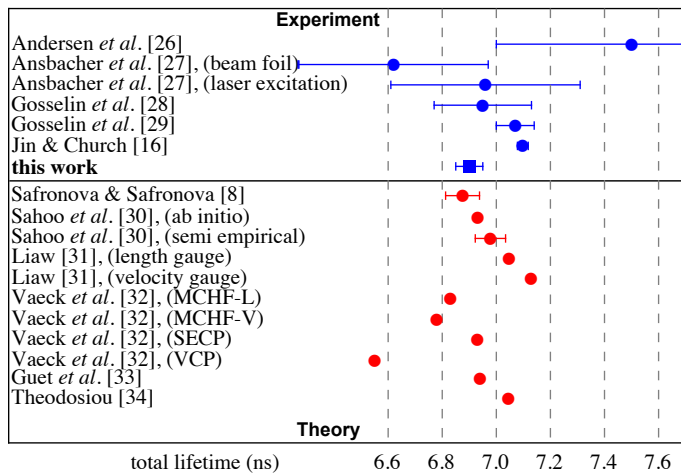


FIG. 4. Comparison of the measured lifetime with theoretical and experimental results for $P_{1/2}$ - level lifetimes from references [8, 16, 26, 27, 28, 29, 30, 31, 32, 33, 34]

Our value for τ is compared to previously reported values in Fig. 4. We find that our value agrees with the latest theory predictions [8], while it is in substantial disagreement with the most recent experimental result [16]. Our value for the branching fraction is in agreement with the results from recent measurements [14]. To our knowledge

TABLE I. List of relative measurement uncertainties for γ_{PS} . Statistical errors are denoted by (*). The shift for the $P_{3/2}$ state depends on Δ , we indicate the average value here. Note that the total error is not the sum of the individual contributions, as statistical and systematic errors are taken into account.

Effect	Shift $\cdot 10^{-3}$	Error $\cdot 10^{-3}$
Residual ϵ_0 polarized light	3.3	2.9
Uncert. of resonance frequency	-	1.6
Stat. uncertainty of δR	-	1.3(*)
Residual near-resonant light	-0.4	0.5
Wavemeter precision	-	0.4(*)
$D_{3/2}$ depletion	0.3	0.2
Uncertainty of Δ_S	-	0.2(*)
Influence of micro motion	-	0.1
Influence of $P_{3/2}$ state	0.3	< 0.1
Residual line-broadening effects	0.1	< 0.1
Total	+3.6	6.8

there is no experimentally determined value of \mathcal{D} so far, where our value is in agreement with the calculation from [8] as well. It is possible to infer the value of the reduced matrix element pertaining to the $4^2S_{1/2} \leftrightarrow 4^2P_{3/2}$ transition, which results to $\sqrt{2}\mathcal{D} = 4.09(1) \text{ ea}_0$. Both reduced dipole matrix elements enter in the calculation of the blackbody-radiation (BBR) shift of the $4^2S_{1/2} \leftrightarrow 3^2D_{3/2}$ and $4^2S_{1/2} \leftrightarrow 3^2D_{5/2}$ quadrupole transitions, which are widely used testbeds for high precision laser spectroscopy [35]. The BBR shift is a major contributor to the uncertainty of clock transition frequencies, for species such as $^{43}\text{Ca}^+$ [36], Al^+ [37] and Sr [38], some of which are used for state-of-the art optical clock experiments and discussed as new SI frequency standards [1, 39, 40]. Our results confirm the validity of computational methods used to predict the BBR shift in such optical clocks. In summary, we demonstrate a novel method for the measurement of dipole matrix elements, which relies on quantum logic techniques and which works in the presence of additional decay channels. We attain a precision and accuracy on the 10^{-3} level. All major error sources can be potentially mitigated, such that measurements of radiative decay rates at unprecedented accuracies in the 10^{-4} regime appear within reach with current technology.

We acknowledge financial support by the European commission within the IP SIQS and by the Bundesministerium für Bildung und Forschung via IKT 2020 (Q.com). We thank Vladan Vuletic, Rene Gerritsma and Marianna Safronova for helpful discussions.

* hettrich@uni-mainz.de

† <http://www.quantenbit.de>

[1] P. O. Schmidt, T. Rosenband, C. Langer, W. M. Itano, J. C. Bergquist, and D. J. Wineland, *Science*, **309**, 749 (2005)

- [2] T. Rosenband, D. B. Hume, P. O. Schmidt, C. W. Chou, A. Bruschi, L. Lorini, W. H. Oskay, R. E. Drullinger, T. M. Fortier, J. E. Stalnaker, S. A. Diddams, W. C. Swann, N. R. Newbury, W. M. Itano, D. J. Wineland, and J. C. Bergquist, *Science*, **319**, 1808 (2008)
- [3] M. S. Safronova, M. G. Kozlov, and C. W. Clark, *Phys. Rev. Lett.*, **107**, 143006 (2011)
- [4] E. Rauscher and G. W. Marcy, *PASP*, **118**, 617 (2006)
- [5] M. Carlsson and J. Leenaarts, *A&A*, **539**, A39 (2012)
- [6] N. Fortson, *Phys. Rev. Lett.*, **70**, 2383 (1993)
- [7] T. W. Koerber, M. H. Schacht, K. R. G. Hendrickson, W. Nagourney, and E. N. Fortson, *Phys. Rev. Lett.*, **88**, 143002 (2002)
- [8] M. S. Safronova and U. I. Safronova, *Phys. Rev. A*, **83**, 012503 (2011)
- [9] C. D. Herold, V. D. Vaidya, X. Li, S. L. Rolston, J. V. Porto, and M. S. Safronova, *Phys. Rev. Lett.*, **109**, 243003 (2012)
- [10] S. Olmschenk, D. Hayes, D. N. Matsukevich, P. Maunz, D. L. Moehring, K. C. Younge, and C. Monroe, *Phys. Rev. A*, **80**, 022502 (2009)
- [11] K. Beloy, J. A. Sherman, N. D. Lemke, N. Hinkley, C. W. Oates, and A. D. Ludlow, *Phys. Rev. A*, **86**, 051404 (2012)
- [12] J. Hartmann, *Astrophysical Journal*, **19**, 268 (1904)
- [13] R. Gerritsma, G. Kirchmair, F. Zähringer, J. Benhelm, R. Blatt, and C. F. Roos, *Eur. Phys. J. D*, **50**, 13 (2008)
- [14] M. Ramm, T. Pruttivarasin, M. Kokish, I. Talukdar, and H. Häffner, *Phys. Rev. Lett.*, **111**, 023004 (2013)
- [15] A. Kreuter, C. Becher, G. P. T. Lancaster, A. B. Mundt, C. Russo, H. Häffner, C. Roos, W. Hänsel, F. Schmidt-Kaler, R. Blatt, and M. S. Safronova, *Phys. Rev. A*, **71**, 032504 (2005)
- [16] J. Jin and D. A. Church, *Phys. Rev. Lett.*, **70**, 3213 (1993)
- [17] D. Leibfried, R. Blatt, C. Monroe, and D. Wineland, *Rev. Mod. Phys.*, **75**, 281 (2003)
- [18] U. G. Poschinger, G. Huber, F. Ziesel, M. Deiss, M. Hettrich, S. A. Schulz, G. Poulsen, M. Drewsen, R. J. Hendricks, K. Singer, and F. Schmidt-Kaler, *J. Phys. B: At. Mol. Opt. Phys.*, **42**, 154013 (2009)
- [19] R. Grimm and M. Weidemüller, *Adv. At. Mol. Opt. Phys.*, **42**, 95 (2000)
- [20] D. J. Wineland, M. Barret, J. Britton, J. Chiaverini, B. DeMarco, W. M. Itano, B. Jelenkovic, C. Langer, D. Leibfried, V. Meyer, T. Rosenband, and T. Schätz, *Phil. Trans. R. Soc. Lond. A.*, **361**, 1349 (2003)
- [21] D. Leibfried, B. DeMarco, V. Meyer, D. Lucas, M. Barrett, J. Britton, W. M. Itano, B. Jelenkovic, C. Langer, T. Rosenband, and D. J. Wineland, *Nature*, **422**, 412 (2003)
- [22] R. Ozeri, C. Langer, J. D. Jost, B. DeMarco, A. Ben-Kish, B. R. Blakestad, J. Britton, J. Chiaverini, W. M. Itano, D. B. Hume, D. Leibfried, T. Rosenband, P. O. Schmidt, and D. J. Wineland, *Phys. Rev. Lett.*, **95**, 030403 (2005)
- [23] H. Uys, M. J. Biercuk, A. P. VanDevender, C. Ospelkaus, D. Meiser, R. Ozeri, and J. J. Bollinger, *Phys. Rev. Lett.*, **105**, 200401 (2010)
- [24] S. Schulz, U. Poschinger, F. Ziesel, and F. Schmidt-Kaler, *New J. Phys.*, **10**, 045007 (2008)
- [25] C. Wunderlich, T. K. Th. Hannemann and, H. Häffner, C. Roos, W. Hänsel, R. Blatt, and F. Schmidt-Kaler, *J. Mod. Opt.*, **54**, 1541 (2007)
- [26] T. Andersen, J. Desesquelles, K. A. Jessen, and G. Sørensen, *J. Quant. Spectrosc. Radiat. Transfer*, **10**, 1143 (1970)
- [27] W. Ansbacher, A. S. Inamdar, and E. H. Pinnington, *Phys. Lett.*, **110A**, 383 (1985)
- [28] R. N. Gosselin, E. H. Pinnington, and W. Ansbacher, *Nuc. Inst. Meth. B*, **31**, 305 (1988)
- [29] R. N. Gosselin, E. H. Pinnington, and W. Ansbacher, *Phys. Rev. A*, **38**, 4887 (1988)
- [30] B. K. Sahoo, B. P. Das, and D. Mukherjee, *Phys. Rev. A*, **79**, 052511 (2009)
- [31] S.-S. Liaw, *Phys. Rev. A*, **51**, R1723 (1995)
- [32] N. Vaeck, M. Godefroid, and C. Froese Fischer, *Phys. Rev. A*, **46**, 3704 (1992)
- [33] C. Guet and W. R. Johnson, *Phys. Rev. A*, **44**, 1531 (1991)
- [34] C. E. Theodosiou, *Phys. Rev. A*, **39**, 4880 (1989)
- [35] M. Chwalla, J. Benhelm, K. Kim, G. Kirchmair, T. Monz, M. Riebe, P. Schindler, A. S. Villar, W. Hänsel, C. F. Roos, R. Blatt, M. Abgrall, G. Santarelli, G. D. Rovera, and P. Laurent, *Phys. Rev. Lett.*, **102**, 023002 (2009)
- [36] B. Arora, M. S. Safronova, and C. W. Clark, *Phys. Rev. A*, **76**, 064501 (2007)
- [37] M. S. Safronova, M. G. Kozlov, and C. W. Clark, *IEEE Transactions on Ultrasonics, Ferroelectrics, and Frequency Control*, **59**, 439 (2012)
- [38] M. S. Safronova, S. G. Porsev, U. I. Safronova, M. G. Kozlov, and C. W. Clark, *Phys. Rev. A*, **87**, 012509 (2013)
- [39] C. W. Chou, D. B. Hume, J. C. J. Koelemeij, D. J. Wineland, and T. Rosenband, *Phys. Rev. Lett.*, **104**, 070802 (2010)
- [40] B. J. Bloom, T. L. Nicholson, J. R. Williams, S. L. Campbell, M. Bishof, X. Zhang, W. Zhang, S. L. Bromley, and J. Ye, *Nature*, **506**, 71 (2014)

Measurement of dipole matrix elements with a single trapped ion: Supplemental material

M. Hettrich^{*1}, T. Ruster¹, H. Kaufmann¹, C. F. Roos^{2,3}, C. T. Schmiegelow¹, F. Schmidt-Kaler¹, and U. G. Poschinger¹

¹QUANTUM, Institut für Physik, Universität Mainz, Staudingerweg 7, 55128 Mainz, Germany

²Institut für Quantenoptik und Quanteninformation, Österreichische Akademie der Wissenschaften, Technikerstraße 21a, 6020 Innsbruck, Austria

³Institut für Experimentalphysik, Universität Innsbruck, Technikerstraße 25, 6020 Innsbruck, Austria

May 13, 2015

In this document, we present details on how to avoid, suppress and characterize corrections, systematic and statistical errors in our measurement scheme to determine dipole matrix elements. In Sec. 1, we briefly repeat the expressions for the essential quantities for convenience, as many of the corrections and errors discussed below arise from the fact that the expressions in Sec. 1 are approximations. In Sec. 2, we give details on how data for the different quantities was acquired, and numerical values for the resulting quantities are listed. Sec. 3 explains details of the experimental setup and methods which are related to error mitigation. In Sec. 4, we discuss all sources of corrections and errors in detail and list numerical values for these. Finally, in Sec. 6, we give ideas on how the error sources can be suppressed by refinements of the experimental techniques.

Contents

1 Prerequisites	2
2 Measurements to determine γ_{PS}, γ_{PD} and τ	3
3 Experimental considerations	4
3.1 Post-selection	4
3.2 Pulse area stability	4
3.3 State preparation and readout (SPAM) errors	5

^{*}hettrich@uni-mainz.de

4	Uncertainties and corrections of the measured variables	5
4.1	Statistical Uncertainty of δR and b	5
4.2	Detuning Δ	6
4.3	Residual near-resonant light at 397 nm	7
4.4	Residual π -polarized scattering light	8
4.5	Differential Stark Shift Δ_S	9
4.6	Zeeman shift	9
4.7	Influence of Micromotion	10
4.8	Influence of near-resonance-effects	10
4.9	Finite $D_{3/2}$ -lifetime and residual 866 nm repump light	11
4.10	Influence of the $P_{3/2}$ state	12
4.11	Fit bias	13
4.12	SPAM errors	13
5	Total uncertainties and corrections of γ_{PS}, γ_{PD} and τ	13
6	Prospects for error mitigation	14

1 Prerequisites

Our measurement scheme is based on the assumption that the ac Stark shift generated by the off-resonant beam is given by the expression

$$\Delta_S = \frac{1}{3} \frac{\Omega^2}{4\Delta} (\epsilon_-^2 - \epsilon_+^2), \quad (1)$$

and the corresponding spin-flip rates are given by:

$$R_{\pm} = \gamma_{PS} \frac{\epsilon_{\pm}^2 + \epsilon_0^2}{9} \frac{\Omega^2}{4\Delta^2}, \quad (2)$$

and correspondingly for decay into the $D_{3/2}$ state:

$$R_{\uparrow(\downarrow)D} = 3(\gamma_{PD}/\gamma_{PS})R_{-(+)}. \quad (3)$$

We describe the population redistribution by the rate equations:

$$\begin{aligned} \dot{p}_{\uparrow} &= -R_-(1+b)p_{\uparrow} + R_+p_{\downarrow} \\ \dot{p}_{\downarrow} &= -R_+(1+b)p_{\downarrow} + R_-p_{\uparrow}. \end{aligned} \quad (4)$$

This allows us to deduce the radiative decay rate from measured quantities:

$$\gamma_{PS} = 3\Delta \frac{\delta R}{\Delta_S}, \quad (5)$$

2 Measurements to determine γ_{PS} , γ_{PD} and τ

According to Eq. 5, the natural linewidth γ_{PS} is determined by the detuning from resonance Δ , the differential ac Stark shift Δ_S and the differential scattering rate δR . These quantities have been measured as follows:

- Detuning Δ :

The detuning Δ_R is determined by measuring the absolute frequency f_j of the scattering light for each detuning j . The number of detunings $D = 4$ (two on the blue side and two on the red side of the resonance) and the resonance frequency f_{res} of the $S - P$ -transition, which is determined as described in section 4.2.

- Scattering rates R_+ and R_-

We have acquired a total number of 65 scattering curve pairs, distributed among four detunings Δ_i , such that for each detuning $N_i = \{18, 17, 14, 16\}$ measurements were done. Each pair consists of one curve for initialization in $|\uparrow\rangle$, and one in $|\downarrow\rangle$. For each of these data sets, 30 different pulse times when the off-resonant beam is switched on were probed, ranging between 0 ms and 1 ms. The pulse times are unevenly distributed along the time axis to provide a more dense sampling for short pulse times. The 30 pulse times are probed in chunks of 25 repetitions, in a random permutation to avoid systematic effects. This is repeated 100 times, such that in total 2500 interrogations per pulse time are performed. For zero pulse time, in total 5000 interrogations are performed, which allows for a better accuracy in the determination of the readout parameters, c.f. Sec. 3.3. The measurements for each initialization level are performed within one sequence.

The polarization of the off-resonant light is adjusted to be predominantly σ^+ , i.e. $R_+ \gg R_-$, and it is not changed throughout all measurements. The two curves of each curve pair are *jointly* fitted to the model function. The fit provides the values $R_{+,i,j}$ and $R_{-,i,j}$ for curve pair (i, j) . j identifies the detuning, and i identifies the number of measurement for that respective detuning.

- Differential Stark shift Δ_S

For each scattering curve pair (i, j) , right before and right after the scattering measurement, Stark shift measurements are carried out, the mean of which, $\Delta_{S,i,j}$, is considered to be the Stark shift belonging to measurement (i, j) .

For each scattering curve pair, $\gamma_{PS,i,j}$ is calculated. We take the mean of those, and arrive at:

$$\gamma'_{PS} = 2\pi \times 21.48 \text{ MHz} \quad (6)$$

Taking into account all corrections from section 4, that value reads:

$$\gamma_{PS} = 2\pi \times 21.57 \text{ MHz} \quad (7)$$

For each measured scattering curves (i, j) , the branching parameter $b_{i,j}$ is also given by the same fit mentioned above. With the mean of all $b_{i,j}$, b , the natural linewidths γ_{PS} and γ_{PD} are related as follows:

$$\gamma_{PD} = \frac{b}{3}\gamma_{PS} = 2\pi \times 1.48 \text{ MHz} \quad (8)$$

The total lifetime of the $P_{1/2}$ -state τ is finally:

$$\tau = \frac{1}{\gamma_{PS} + \gamma_{PD}} = 6.90 \text{ ns} \quad (9)$$

The resulting values for these quantities are shown in table 2. The numbers are given for the four detunings Δ_i , each averaged over the N_i respective datasets.

i	$\Delta_i/2\pi$ (GHz)	$R_{i,+}$ (s^{-1})	$R_{i,-}$ (s^{-1})	$\Delta_{S,i}/2\pi$ (MHz)	b_i	$\gamma_{PS,i}/2\pi$ (MHz)
1	-13.94	4474(78)	47(7)	1.3753	0.2063(48)	21.45(33)
2	-12.03	6011(80)	63(11)	1.58819	0.2080(53)	21.52(30)
3	11.52	6514(125)	101(7)	1.64198	0.2056(45)	21.49(39)
4	13.42	4762(40)	76(8)	1.39819	0.2067(52)	21.48(17)

3 Experimental considerations

3.1 Post-selection

The data is post-selected in such a way that chunks of 25 interrogations where the ion is not found sufficiently bright after reset - indicating an impairment of Doppler cooling - are discarded. Similarly, chunks where the shelving was impaired were discarded, which can be identified by spuriously low dark count fractions. In total, less than 1% of all raw datapoints have been removed by this post-selection scheme.

3.2 Pulse area stability

Our measurement scheme relies on a constant optical power and polarization from the off-resonant laser near 397 nm at the location of the trapped ion. Several measures are employed to guarantee the stability. The laser light derived from a doubled, amplified laser system (Toptica TA-SHGpro) is coupled into a single mode fiber. At the fiber output, a polarizer filters undesired polarization components. After the polarizer, a small fraction of the optical power is picked and measured on a photodetector. The signal is used by a commercial intensity stabilization unit (NoiseEater, TEM Messtechnik), which acts on an electro-optical modulator before the fiber input. This way, intensity *and* polarization after the fiber output are actively stabilized. For switching, we employ an acousto-optical modulator (AOM)¹, which exhibits no measureable² beam pointing drift when switching between no power and maximum rf-power (2 W). The rf amplifier supplying the AOM is mounted on a temperature-stabilized water-cooled plate to avoid temperature-change-induced power drifts. The laser beam is focused such that zero and higher diffraction orders coincide at the position of the trapped ion, i.e. residual AOM induced beam pointing fluctuations are mitigated. Further mitigation is ensured by a relatively large beam waist of about 30 μm , and a careful positioning of the ion at the waist center by maximizing the ac Stark shift. Diffraction angle and efficiency of an AOM weakly depends its temperature, and thus on the time-averaged rf-power. This is kept constant by fixing all pulse sequences for measurement of the ac Stark shifts and scattering rates to the same duration, and inserting additional rf pulses after readout to keep the average switched-on time constant.

¹I-M110-3C10BB-3-GH27, Gooch&Housego

²Measured with a position sensitive detector PDP90A, Thorlabs

3.3 State preparation and readout (SPAM) errors

Taking into account imperfect initialization, the experimental signals for the scattering rate measurements are modeled by a linear transformation of the populations from Eq. 4:

$$\begin{aligned} p_{\uparrow}^{(\uparrow)}(t) &= \epsilon_{\downarrow} + (1 - \epsilon_{\uparrow}) \left(a_{\uparrow} \tilde{p}_{\uparrow}^{(\uparrow)}(t) + (1 - a_{\uparrow}) \tilde{p}_{\uparrow}^{(\downarrow)}(t) \right) \\ p_{\uparrow}^{(\downarrow)}(t) &= \epsilon_{\downarrow} + (1 - \epsilon_{\uparrow}) \left(a_{\downarrow} \tilde{p}_{\uparrow}^{(\downarrow)}(t) + (1 - a_{\downarrow}) \tilde{p}_{\uparrow}^{(\uparrow)}(t) \right), \end{aligned} \quad (10)$$

where the $a_{\uparrow} \lesssim 1$ and $a_{\downarrow} \gtrsim 0$ characterize the state preparation (pumping) fidelity, ϵ_{\downarrow} (ϵ_{\uparrow}) is the error probability that the ion is spuriously detected as being in state $|\uparrow\rangle$ ($|\downarrow\rangle$), when it actually is in state $|\downarrow\rangle$ ($|\uparrow\rangle$).

4 Uncertainties and corrections of the measured variables

We carefully distinguish statistical and systematic errors, and systematic shifts. A statistical error of a given quantity is denoted by $\epsilon(\cdot)$, while a systematic error is denoted by $\sigma(\cdot)$. A systematic shift is denoted by $\delta(\cdot)$, and it is accompanied by a systematic error. All shifts and uncertainties are reported as *relative* quantities. Some error sources are found to be small as compared to the dominating ones, in this case an estimation of the magnitude is given, however these error sources are not quantitatively taken into account in the total error. If this is the case, it is explicitly stated in the corresponding section. As our total error is on the 10^{-3} level, we do not take corrections and errors below the 10^{-4} level into account in the final error budget. In the cases where we report mean values $\bar{\epsilon}, \bar{\sigma}$, these quantities result from averaging over all data sets. In these cases, the individual values for each data-set rather than the indicated mean values are used for the computation of the final values.

4.1 Statistical Uncertainty of δR and b

For each curve i , $R_{\pm, i, j}$ and b are determined by a fit of the depolarization data to the model Eqs. 10. The uncertainties of that fit are extracted by marginalization of the data generated by the used Markov Chain Monte Carlo algorithm. It is verified by parametric bootstrapping: For fixed R_{\pm} and b values, 30 instances of simulated measurement data with binomial noise are generated and fitted in the same way as the original data, each fit yielding result values for R_{\pm} and b and their statistical errors. The standard errors determined from the actual data are in agreement with the standard deviation of the mean values found for the 30 bootstrapping datasets. Note that cross-correlations between uncertainties of R_{\pm} and b and the additional parameters introduced for characterizing SPAM errors, c.f. Sec. 3.3, are fully taken into account due to the marginalization of the Monte Carlo data.

The individual standard error of δR for each dataset i, j is used to determine the total uncertainty of γ_{PS} , see section 5. The individual standard errors of b affect the total uncertainty Γ_{PD} and τ , c.f. Eqs. 8 and 9. The means over all datasets of the relative statistical errors are

$$\begin{aligned} \bar{\epsilon}(\delta R) &= 12.1 \cdot 10^{-3} \\ \bar{\epsilon}(b) &= 24.8 \cdot 10^{-3} \end{aligned} \quad (11)$$

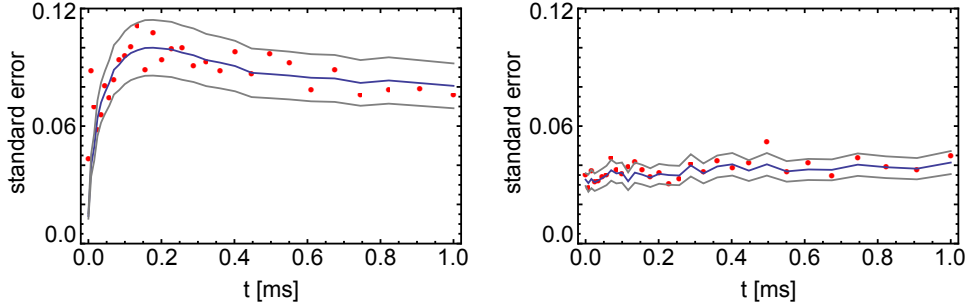


Figure 1: Comparison of expected and actual spreads of measured dark count fractions: We plot the expected population standard deviation Eq. 12 (solid black line), computed using the total estimated dark count fractions $p_{\uparrow}^{(\downarrow, \uparrow)}(t)$ and $N = 25$. The red points are the sample standard deviations of the dark count fractions from the 100 different acquired chunks of $N = 25$ interrogations. The solid grey lines show 2σ intervals for the expected standard sample deviations. A significant fraction of outliers would indicate additional drifts and fluctuations. The data for $p_{\uparrow}^{(\downarrow)}(t)$ is shown in the left panel, the data for $p_{\uparrow}^{(\uparrow)}(t)$ in the right panel.

The validity of the statistical errors relies on the assumption that their dominant source is the readout shot noise of the spin measurements. Possible drifts or fluctuations of the optical power or polarization during a depolarization rate measurement would corrupt this assumption. We verified that no such effects are present on a significant level in the following way: For a given data-set, for each exposure time t , the measurement data for $p_{\uparrow}^{(\uparrow, \downarrow)}(t)$ was taken in chunks comprised of $N = 25$ spin interrogations. For each chunk, coarse estimates for $p_{\uparrow}^{(\uparrow, \downarrow)}(t)$ are obtained by dividing the number of dark count events by the number of interrogations N . The sample standard deviation of these values over the set of chunks is compared to the expected population standard deviation for binomial statistics,

$$\epsilon \left(p_{\uparrow}^{(\uparrow, \downarrow)}(t) \right) = \sqrt{p_{\uparrow}^{(\uparrow, \downarrow)}(t) \left(1 - p_{\uparrow}^{(\uparrow, \downarrow)}(t) \right) / N}. \quad (12)$$

The results are in agreement with the assumption of binomial statistics, we can therefore exclude additional drifts and fluctuations at a significant level. An example is shown in Fig. 1.

4.2 Detuning Δ

The detuning reads $\Delta_j = f_j - f_{res}$, with f_{res} being the so far unknown resonance frequency of the transition. The frequencies f_j are directly recorded by a wavelength meter³. No considerable drifts are recorded, however fluctuations are present. These amount to:

³WSU, High Finesse GmbH

$$\epsilon_{wm}(\Delta_1) = 0.4 \cdot 10^{-3} \quad (13)$$

$$\epsilon_{wm}(\Delta_2) = 0.5 \cdot 10^{-3} \quad (14)$$

$$\epsilon_{wm}(\Delta_3) = 0.6 \cdot 10^{-3} \quad (15)$$

$$\epsilon_{wm}(\Delta_4) = 0.4 \cdot 10^{-3} \quad (16)$$

$$(17)$$

To determine the resonance frequency f_{res} , we note that the ratio of ac Stark shift and differential scattering rate is proportional to the detuning:

$$(-) \frac{1}{3} \frac{\Delta_{S,i,j}}{\delta R_{i,j}} \propto \Delta_j. \quad (18)$$

The minus sign holds for negative detunings. We perform a linear regression of this quantity with respect to the wavelength meter frequency f_j from which the zero-crossing f_{res} , i.e. the resonance frequency, is obtained. The absolute uncertainty of f_{res} is obtained from the linear regression. As f_{res} is used to compute *all* detunings, it is a systematic error. The values are:

$$\sigma_{fit}(\Delta_1) = 1.5 \cdot 10^{-3} \quad (19)$$

$$\sigma_{fit}(\Delta_2) = 1.8 \cdot 10^{-3} \quad (20)$$

$$\sigma_{fit}(\Delta_3) = 1.8 \cdot 10^{-3} \quad (21)$$

$$\sigma_{fit}(\Delta_4) = 1.6 \cdot 10^{-3} \quad (22)$$

$$(23)$$

4.3 Residual near-resonant light at 397 nm

Two laser sources provide spurious residual light weakly driving the cycling transition.

- Doppler cooling laser: The laser used for Doppler cooling and fluorescence readout is switched by an acousto-optical modulator ⁴ in double-pass configuration. An estimate of the residual photon scattering rate due to imperfect switch-off is obtained by initializing the qubit in $|\uparrow\rangle$ or $|\downarrow\rangle$, either before or after a 10 ms wait time before readout. This yields spurious spin flip rates of $R_-^{(res)} = 1.1(6)$ Hz and $R_+^{(res)} = 0.7(4)$ Hz. These rates are taken into account for two of the acquired datasets, by modifying the model Eqs.4, incorporating the fact that these persist throughout the entire 1 ms interval. From fitting with the modified model, obtain the following corrections:

$$\begin{aligned} \delta_{397}(\delta R) &= -4.1 \cdot 10^{-4} \\ \delta_{397}(b) &= -8.3 \cdot 10^{-4} \end{aligned} \quad (24)$$

and systematic errors

$$\begin{aligned} \sigma_{397}(\delta R) &= 4.6 \cdot 10^{-4} \\ \sigma_{397}(b) &= 6.4 \cdot 10^{-4} \end{aligned} \quad (25)$$

⁴I-M110-3C10BB-3-GH27, Gooch&Housego

- Off-resonant laser: The off-resonant light near 397 nm is obtained from an amplified, frequency doubled diode laser system⁵. The amplified fundamental beam seeding the doubler has a broad background of amplified spontaneous emission (ASE), extending over about 30 nm, equivalent to $\delta_{amp} \approx 2\pi \cdot 57$ THz. The suppression with respect to the coherent light is specified to be $\chi = -40$ dB. One might argue that this background leads to additional UV light near the atomic resonance, which would effectively shorten the measured lifetime. We give a pessimistic estimate of this effect, assuming only $\chi = -30$ dB ASE suppression, perfect phase-matching for sum-frequency generation (SFG) of ASE and laser mode photons, perfect AOM diffraction even for incoherent light and that a spurious component exactly hits the atomic resonance. With a SHG cavity linewidth of $\delta_c = 2\pi \cdot 500$ kHz, we obtain a power ratio of the spurious to the main SHG component of

$$\frac{P_{spur}}{P_{SHG}} \approx \chi \frac{\delta_c}{\delta_{amp}} \approx 9 \cdot 10^{-15} \quad (26)$$

This strong suppression even under pessimistic assumptions leads us to the conclusion that this effect does not have to be taken into account. We still perform an experimental verification, where we probe depolarization after initialization in $|\downarrow\rangle$, at a fixed off-resonant pulse-time of 50 μ s, corresponding to about 20% depolarization. We scan the laser frequency over a range of 1.3 GHz, which is more than one free spectral range of the SHG cavity. The scan speed about 2 MHz/s, such that one data point integrates over about 4 MHz, which is slow enough to resolve the atomic line. No resonant features were observed in the resulting depolarization signal.

4.4 Residual π -polarized scattering light

The k-vector of the scattering light is aligned parallel to the magnetic field, so ideally only σ -transitions can be driven. Alignment errors of the beam might be the cause for residual π -polarized light, which is not accounted for in Eq. 3. Taking into account an the pumping to the $D_{3/2}$ caused by additional π polarized light, the rate equations Eqs. 4 are extended, including an additional parameter R_D :

$$\begin{aligned} \dot{p}_\uparrow &= -R_-(1+b)p_\uparrow - R_D p_\uparrow + R_+ p_\downarrow \\ \dot{p}_\downarrow &= -R_+(1+b)p_\downarrow - R_D p_\downarrow + R_- p_\uparrow. \end{aligned} \quad (27)$$

with

$$R_D = \frac{b \epsilon_0^2}{2 \epsilon_+^2} R_+. \quad (28)$$

The solutions of the rate equations are of the same form as for Eq. 4, however with altered coefficients

$$\bar{R} = (1+b)(R_- + R_+) + R_D \quad (29)$$

$$\tilde{R}^2 = \bar{R}^2 - 4(2+b)(R_D + bR_-)R_+. \quad (30)$$

If the data is now fitted using this modified model, we obtain values of about $R_D = 3(3)$ Hz, and altered values for $\delta R, b$. The mean value of the deviations of $\delta R, b$ are used to compute the corrections:

$$\begin{aligned} \bar{\delta}_\pi(\delta R) &= 3.3 \cdot 10^{-3} \\ \bar{\delta}_\pi(b) &= -2.4 \cdot 10^{-3}, \end{aligned} \quad (31)$$

⁵TA SHGpro, Toptica Photonics AG

and the spread of the deviations within each data-set determines the systematic error

$$\begin{aligned}\bar{\sigma}_\pi(\delta R) &= 2.9 \cdot 10^{-3} \\ \bar{\sigma}_\pi(b) &= 2.6 \cdot 10^{-3}\end{aligned}\tag{32}$$

4.5 Differential Stark Shift Δ_S

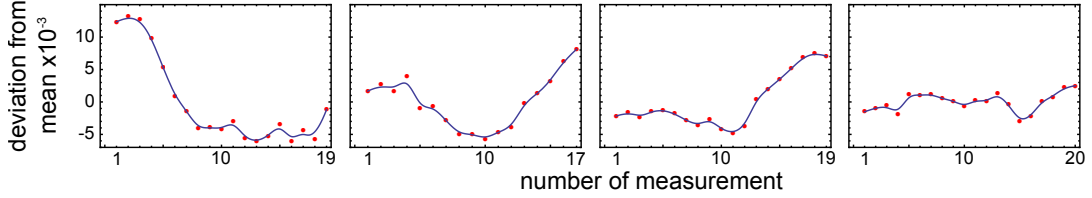


Figure 2: The red points depict the relative deviations of the ac Stark shift values $\Delta_{S,i,j}$ from their mean for all four measurement sessions. The blue curves are the B-spline functions defined by the points. The RMS deviation of the points from the spline is used as the statistical error.

We carried out the bootstrapping method from Sec. 4.1 for determining the uncertainty of the ac Stark Shift Δ_S . The result is that the uncertainty from the binomial readout statistics of the measurement would lead to insignificant uncertainties on the 10^{-7} level. Systematic effects, i.e. temporal drifts, are clearly dominant.

$\Delta_{S,i,j}$ is for each dataset i, j is determined by the mean of two measurements, taken before and after the scattering rate measurement yielding $\delta R_{i,j}$. The drift of the ac Stark shift drift over the measurement time each detuning Δ_i is slow and therefore mostly resolved, thus the assumption of a linear drift between two consecutive stark shift measurements is justified. To account for residual drifts on a timescale which is not resolved, we use the measured Δ_S values as control points to define a B-spline function as shown in Fig. 2. The RMS of the difference of the measurement result and the corresponding B-spline value is treated as the overall inaccuracy $\epsilon(\Delta_{S,i,j})$ of all Δ_S values pertaining to detuning Δ_i . The mean value of those relative uncertainties reads

$$\bar{\epsilon}(\Delta_S) = 3.0 \cdot 10^{-4}\tag{33}$$

4.6 Zeeman shift

We do not take the Zeeman shifts of the atomic levels ($\Delta_Z = 2\pi \cdot 13.34$ MHz splitting between $|\uparrow\rangle$ and $|\downarrow\rangle$) into account. However, as the atomic resonance frequency is determined via the ac Stark shift caused by the predominantly σ_+ polarized beam, the detuning Δ specifically refers to the $|S_{1/2}, m_J = -1/2\rangle \leftrightarrow |P_{1/2}, m_J = +1/2\rangle$ transition *including* its Zeeman shift. Corrections are only necessary for the transitions driven by the weak σ_- and π polarization components. The corresponding systematic errors are estimated to be

$$\begin{aligned}\sigma_Z(\delta R) &\approx \frac{\epsilon_{0,-}^2}{\epsilon_+^2} \frac{\Delta_Z}{\Delta} \approx \frac{R_-}{R_+} \frac{\Delta_Z}{\Delta} \lesssim 3 \cdot 10^{-5} \\ \sigma_Z(\Delta_S) &\lesssim 2 \cdot 10^{-5}\end{aligned}\tag{34}$$

4.7 Influence of Micromotion

Both the scattering rates R_+ , R_- and the Stark shift Δ_S are altered in the presence of micromotion along the propagation direction of the off-resonant beam. The micromotion causes effective frequency modulation (FM), characterized by the trap drive frequency $\Omega_{rf} = 2\pi \cdot 25$ MHz and the modulation index β . We obtain

$$R_{\pm}^{(mm)} \approx \gamma_{PS} \frac{\epsilon_{\pm}^2 + \epsilon_0^2}{9} \sum_{n=-\infty}^{+\infty} J_n^2(\beta) \frac{\Omega^2}{4(\Delta + n\Omega_{rf})^2} \quad (35)$$

$$\Delta_S^{(mm)} \approx \frac{\epsilon_+^2 - \epsilon_-^2}{3} \sum_{n=-\infty}^{+\infty} J_n^2(\beta) \frac{\Omega^2}{4(\Delta + n\Omega_{rf})} \quad (36)$$

By measuring the the shape of the resonance fluorescence line by recording fluorescence photons at low power and across resonance, an upper bound for the modulation Index of $\beta = 3.5$ is obtained. Note that the micromotion-induced frequency modulation leads to symmetric FM sidebands, therefore the effects cancel out to first order. Due to the $\Delta^{-1}(\Delta^{-2})$ scaling behavior of the ac Stark shift (scattering rates), *both* quantities are slightly increased by FM components on the side towards the resonance, such that the total effect partially cancels out. Thus, we give an estimate for the systematic error of the resulting γ_{PS} rather than for Δ_S and δR . Using realistic values of Ω^2 , ϵ_+^2 , ϵ_-^2 and Δ , we obtain

$$\sigma_{mm}(\gamma_{PS}) = \frac{1}{\delta R} \left(\delta R^{(mm)} - \delta R \right) - \frac{1}{\Delta_S} \left(\Delta_S^{(mm)} - \Delta_S \right) \approx 1.0 \cdot 10^{-4} \quad (37)$$

4.8 Influence of near-resonance-effects

The expressions for δR Eq. 2 and Δ_S Eq. 1 are only valid if $|\Delta| \gg \gamma_{PS}, \Omega$. Our experimental conditions are $\gamma_{PS}/|\Delta| \lesssim 2 \cdot 10^{-3}$, $\Omega/|\Delta| \lesssim 4 \cdot 10^{-2}$, we therefore investigate how the approximations affect the results.

The *measured*, i.e. actual scattering rate $\delta R^{(meas)}$ is *smaller* than the far-off-resonance approximation Eq. 2. Including power broadening and finite natural linewidth, the scattering rate is given by

$$\begin{aligned} \delta R^{(meas)} &= \gamma_{PS} \frac{\epsilon_+^2 - \epsilon_-^2}{9} \frac{\Omega^2}{4\Delta^2 + \frac{2}{3}\Omega^2 + \gamma_{PS}^2} \\ &\approx \gamma_{PS} \frac{\epsilon_+^2 - \epsilon_-^2}{9} \Omega^2 \left(\frac{1}{4\Delta^2} - \frac{\frac{2}{3}\Omega^2 + \gamma_{PS}^2}{16\Delta^4} \right) \\ &= \delta R + \delta R' \end{aligned} \quad (38)$$

We thus have

$$\delta R' = -\delta R \frac{\frac{2}{3}\Omega^2 + \gamma_{PS}^2}{4\Delta^2} \quad (39)$$

The correction is obtained by invoking the expression Eq. 5 for the decay rate γ_{PS} :

$$\begin{aligned} \gamma_{PS} &= \frac{3\Delta}{\Delta_S} (\delta R^{(meas)} - \delta R') \\ &= \frac{3\Delta}{\Delta_S} \delta R^{(meas)} (1 + \delta_{broad}(\delta R)) \end{aligned} \quad (40)$$

such that

$$\delta_{broad}(\delta R) = -\frac{\delta R'}{\delta R^{(meas)}} \approx 2\Delta_S/\Delta \quad (41)$$

We obtain

$$\begin{aligned} \delta_{broad}(\delta R_1) &= 2.0 \cdot 10^{-4} \\ \delta_{broad}(\delta R_2) &= 2.6 \cdot 10^{-4} \\ \delta_{broad}(\delta R_3) &= 2.9 \cdot 10^{-4} \\ \delta_{broad}(\delta R_4) &= 2.1 \cdot 10^{-4}. \end{aligned} \quad (42)$$

For Δ_S , no expression corresponding to Eq. 38 is available, we therefore extract values from a numerical simulation using a three-level generalized optical Bloch equation. For $\delta_{broad}(\Delta_S) = (\Delta_S^{(meas)} - \Delta_S)/\Delta_S^{(meas)}$, we obtain

$$\begin{aligned} \delta_{broad}(\Delta_{S,1}) &= 1.0 \cdot 10^{-4} \\ \delta_{broad}(\Delta_{S,2}) &= 1.4 \cdot 10^{-4} \\ \delta_{broad}(\Delta_{S,3}) &= 1.4 \cdot 10^{-4} \\ \delta_{broad}(\Delta_{S,4}) &= 1.0 \cdot 10^{-4}. \end{aligned} \quad (43)$$

4.9 Finite $D_{3/2}$ -lifetime and residual 866 nm repump light

In the model Eqs. 4, the lifetime of the $D_{3/2}$ -state is considered to be infinite. The most recent experimental value is 1176(11) ms (Kreuter et. al., PRA 71, 2005). Residual light near 866 nm also depletes population accumulated in the $D_{3/2}$ state at a rate R_{dep} , effectively reducing its lifetime. We measure the residual power in the imperfectly switched off beam, using a fibre-coupled avalanche photodiode, to about 6 pW. In the switched-on state, the optical power is 86 μ W. For observing the amount of resonance fluorescence versus optical power at 866 nm, we infer a saturation parameter of 23(5). This leads to a saturation parameter in the switched-off state of $S_{off}^{(866)} = 1.6(8) \cdot 10^{-6}$. The depletion rate of the $D_{3/2}$ state is then

$$R_{D_{3/2}}^{(dep)} = \frac{\gamma_{PS}}{2} \frac{S_{off}^{(866)}}{1 + 4\bar{\delta}^2/\gamma_{PD}^2}. \quad (44)$$

Here, $\bar{\delta}$ is the average detuning of the sub-transitions between the $P_{1/2}$ and $D_{3/2}$ manifolds, considering the Zeeman splitting (see Sec. 4.6) and the repump laser to be tuned onto the blue side of the entire manifold. We obtain a laser induced depletion rate of 1.2(1.0) Hz. Thus, the $D_{3/2}$ state is depleted at a total rate of about $R_{D_{3/2}}^{(dep)} = 2.2(1.0)$ Hz.

For estimating the impact of the depletion on the result for δR , we modify the rate equations Eqs. 4 to be

$$\begin{aligned} \dot{p}_\uparrow &= -R_-(1+b)p_\uparrow + R_+p_\downarrow + \frac{1}{2}R_{D_{3/2}}^{(dep)}(1-p_\uparrow-p_\downarrow) \\ \dot{p}_\downarrow &= -R_+(1+b)p_\downarrow + R_-p_\uparrow + \frac{1}{2}R_{D_{3/2}}^{(dep)}(1-p_\uparrow-p_\downarrow). \end{aligned} \quad (45)$$

Using these for example data in our fit procedure, we infer the systematic shifts

$$\begin{aligned}\delta_{\gamma D_{3/2}}(\delta R) &= 3.2 \cdot 10^{-4} \\ \delta_{\gamma D_{3/2}}(b) &= 1.6 \cdot 10^{-3}\end{aligned}\tag{46}$$

and systematic errors

$$\begin{aligned}\sigma_{\gamma D_{3/2}}(\delta R) &= 1.6 \cdot 10^{-4} \\ \sigma_{\gamma D_{3/2}}(b) &= 7 \cdot 10^{-4}\end{aligned}\tag{47}$$

4.10 Influence of the $P_{3/2}$ state

The $P_{3/2}$ is separated from the $P_{1/2}$ manifold by the fine-structure-splitting of $\Delta_{FS} \approx 2\pi \cdot 6.69$ THz. The coupling strength Ω^2 is increased with respect to the $P_{1/2}$ state by a factor of 2, given by the ration of the squared reduced dipole matrix elements, which we indicate explicitly. The presence of these levels affects both the Stark-shift and the scattering rates. For the scattering, we approximate the decay rate to be the same as for the ${}^2P_{1/2}$ state, and we take only the predominant σ_+ polarization component into account, and we neglect decay into the $D_{3/2}$ and $D_{5/2}$ states. The additional scattering rate then reads:

$$R_+^{(P_{3/2})} \approx \gamma_{PS} \frac{2}{3} \frac{\epsilon_+^2}{6} \frac{2\Omega^2}{4(\Delta_{FS} - \Delta)^2} \approx \gamma_{PS} \frac{1}{9} \frac{2\Omega^2}{4\Delta_{FS}^2}\tag{48}$$

Note that the for the $P_{3/2}$ state, due to the different Clebsch-Gordan coefficients, the branching ratio of decays with spin-flip to decay without spin-flip is reversed with respect to the $P_{1/2}$ state, however the scattering rate has the same prefactor as in Eq. 2. The excitation channel $S_{1/2}, m_J = +1/2 \rightarrow P_{3/2}, m_J = +3/2$ contributes only to elastic scattering. Interference effects between different pathways do not play a role as the emitted photons are distinguishable either by wavelength or by polarization/emission direction. The correction to the ac Stark shift reads:

$$\Delta_S^{(P_{3/2})} \approx \left(\frac{\epsilon_+^2}{2} - \frac{\epsilon_+^2}{6} \right) \frac{2\Omega^2}{4(\Delta_{FS} - \Delta)} \approx \frac{\epsilon_+^2}{3} \frac{2\Omega^2}{4\Delta_{FS}}\tag{49}$$

For the $P_{3/2}$ state, the transition $S_{1/2}, m_J = +1/2 \rightarrow P_{3/2}, m_J = +3/2$ contributes to the differential ac Stark shift and has a larger Clebsch-Gordan coefficient than the transition $S_{1/2}, m_J = -1/2 \rightarrow P_{3/2}, m_J = +1/2$. The reversed sign has to be accounted for as we only measure absolute values of Δ_S . For $\Delta > 0$, the magnitude of Δ_S is increased, for $\Delta < 0$ it is decreased.

We finally obtain

$$\delta_{P_{3/2}}(\Delta_{S,i,j}) = \frac{\Delta_i}{3\Delta_{FS}} \approx 1.0 \cdot 10^{-3} \frac{\Delta_i}{2\pi \cdot 10 \text{ GHz}}\tag{50}$$

$$\delta_{P_{3/2}}(\delta R_{S,i,j}) = \frac{\Delta_i^2}{3\Delta_{FS}^2} \approx 1.5 \cdot 10^{-6} \left(\frac{\Delta_i}{2\pi \cdot 10 \text{ GHz}} \right)^2\tag{51}$$

Note that the $\delta_{P_{3/2}}(\Delta_{S,i,j})$ depend on the sign of Δ_i . We do not include systematic errors due to the small magnitudes of these corrections.

4.11 Fit bias

Parameter estimation from measurement data might be affected by a systematic bias, depending on the used estimator. We generated artificial measurement data from the model Eq. 4 with fixed values of R_{\pm}, b with binomial errors. We find that for increasing number of measurements, i.e. vanishing noise, the fit results for R_{\pm}, b converges to the preset values. We thus do not take any bias into account in our error budget.

4.12 SPAM errors

For the determination of the differential scattering rate δR , SPAM errors are taken into account by employing the model introduced in Sec. 3.3 for the parameter estimation. The uncertainty of the additional parameters and their cross-correlation with R_{\pm}, b is already taken into account, as the statistical error $\epsilon(\delta R)$ is obtained by marginalizing over the sample data from the Monte Carlo parameter estimation algorithm.

5 Total uncertainties and corrections of γ_{PS}, γ_{PD} and τ

The uncorrected values for γ_{PS} for each detuning Δ_i are obtained from averaging:

$$\begin{aligned}\gamma'_{PS,i} &= \frac{1}{N_i} \sum_{j=1}^{N_i} 3\Delta_i \frac{\delta R_{i,j}}{\Delta_{S,i,j}} \\ b'_i &= \frac{1}{N_i} \sum_{j=1}^{N_i} b_{i,j}\end{aligned}\quad (52)$$

The corrected values are obtained by adding all relative corrections:

$$\begin{aligned}\gamma_{PS,i}/\gamma'_{PS,i} &= 1 + \delta_{397}(\delta R) + \delta_{broad}(\delta R_i) + \delta_{\gamma_{D3/2}}(\delta R) + \delta_{\pi}(\delta R) \\ &\quad - \delta_{broad}(\Delta_{S,i}) - \delta_{P3/2}(\Delta_{S,i}) \\ b_i/b'_i &= 1 + \delta_{397}(b) + \delta_{\gamma_{D3/2}}(b) + \delta_{\pi}(b)\end{aligned}\quad (53)$$

The statistical errors are obtained from error propagation:

$$\begin{aligned}\epsilon(\gamma_{PS,i,j})^2 &= \epsilon(\Delta_i)^2 + \epsilon(\Delta_{S,i,j})^2 + \epsilon(\delta R_{i,j})^2 \\ \epsilon(b_i)^2 &= \frac{1}{N_i^2} \sum_{j=1}^{N_i} \epsilon(b_{i,j})^2\end{aligned}\quad (54)$$

The systematic errors are given by

$$\begin{aligned}\sigma(\gamma_{PS,i}) &= \sigma_{mm}(\gamma_{PS}) + \sigma_{fit}(\Delta_i) + \sigma_{397}(\delta R) + \sigma_{\gamma_{D3/2}}(\delta R) + \sigma_{\pi}(\delta R) \\ \sigma(b_i) &= \sigma_{397}(b) + \sigma_{\gamma_{D3/2}}(b) + \sigma_{\pi}(b)\end{aligned}\quad (55)$$

The final values are obtained by a weighted average over the four results:

$$\begin{aligned}\gamma_{PS} &= \frac{1}{\sum_i N_i} \sum_i N_i \gamma_{PS,i} \\ b &= \frac{1}{\sum_i N_i} \sum_i N_i b'_i\end{aligned}\tag{56}$$

The total statistical errors are given by

$$\begin{aligned}\epsilon(\gamma_{PS})^2 &= \frac{1}{(\sum_i N_i)^2} \sum_{i,j} \epsilon(\gamma_{PS,i,j})^2 \\ \epsilon(b)^2 &= \frac{1}{(\sum_i N_i)^2} \sum_i N_i^2 \epsilon(b_i)^2,\end{aligned}\tag{57}$$

and the total systematic errors by

$$\begin{aligned}\sigma(\gamma_{PS}) &= \frac{1}{\sum_i N_i} \sum_i N_i \sigma(\gamma_{PS,i}) \\ \sigma(b) &= \frac{1}{\sum_i N_i} \sum_i N_i \sigma(b_i),\end{aligned}\tag{58}$$

For the radiative decay rate to the $D_{3/2}$ state, $\gamma_{PD} = (b/3)\gamma_{PS}$, we thus have

$$\begin{aligned}\epsilon(\gamma_{PD})^2 &= \epsilon(b)^2 + \epsilon(\gamma_{PS})^2 \\ \sigma(\gamma_{PD}) &= \sigma(b) + \sigma(\gamma_{PS}),\end{aligned}\tag{59}$$

and correspondingly for the total lifetime $\tau = 1/(\gamma_{PS} + \gamma_{PD})$:

$$\begin{aligned}\epsilon(\tau)^2 &= \epsilon(\gamma_{PS})^2 + \frac{b^2}{(3+b)^2} \epsilon(b)^2 \\ \sigma(\tau) &= \sigma(\gamma_{PS}) + \frac{b}{3+b} \sigma(b).\end{aligned}\tag{60}$$

6 Prospects for error mitigation

In the following, we present ideas how the relevant error sources could be mitigated, which would pave the way for measurements of radiative decay rates and lifetimes with unprecedented accuracy in the 10^{-4} or even in the 10^{-5} regime, which is beyond the accuracy of current methods for atomic structure calculation.

In general, many systematic shifts and errors scale with the inverse detuning $1/\Delta$ and can therefore be suppressed by utilizing more laser power and detuning further from resonance. Some other errors scale with the inverse maximum time of the depolarization measurement, which is 1 ms in our case. These errors can thus also be suppressed with more laser power, however the timescale mismatch between the measurement of Δ_S and δR then becomes a problem. A possible solution is to perform a proper calibration of the pick-up laser power, as it is used for the intensity stabilization unit, e.g. by measuring

the ac Stark shift. Then, one could perform the ac Stark shift measurement at much lower optical power than the depolarization rate measurement. This would allow to perform the two measurement at similar timescales, even for much faster depolarization rates.

- Statistical uncertainty of δR and b : The precision of the δR values is determined by the amount of measurement data. Due to the binomial noise, the statistical uncertainty will scale as $1/\sqrt{N}$ for N dichotomic measurements. The acquisition of substantially larger data sets can be achieved by reducing the time requirement for each experimental duty cycle (currently about 5 ms). Accurate readout of qubits in the 10 μ s regime has been demonstrated for trapped ions, and the depolarization rate can be increased by using more optical power. Furthermore, the precision of δR for a given N can be optimized by tailoring the distribution of measurement points along the time axis, e.g. by a Bayesian experiment design technique.
- Detuning Δ : The accuracy of the detuning values are limited by the accuracy of the wavelength meter, and by the accuracy of the determination of the resonance frequency from measured Δ_S and δR values. The frequency measurement could be performed at virtually arbitrary accuracy by employing a frequency comb, and the resonance frequency can be determined more accurately by using larger detunings.
- Residual π -polarized scattering light: A possible refinement of the experimental technique would be to measure the light-induced energy shift individually for the levels $|\uparrow\rangle$ and $|\downarrow\rangle$, by employing the optical transitions to the metastable $D_{5/2}$ state. This would allow for extracting quantitative information on the polarization components $\epsilon_0^2, \epsilon_{\pm}^2$, which can then be fully taken into account.
- Differential ac Stark shift Δ_S : The accuracy of the ac Stark shift values is on the one hand limited by thermal drifts of components of the intensity stabilization system and thermal drifts of the acousto-optical modulator controlling the off-resonant beam and the amplifier of its rf supply. On the other hand, slow beam pointing drifts might affect the accuracy on a similar level. Both error sources can be mitigated by increasing the robustness of the setup against temperature drifts. The beam pointing error can be additionally mitigated by increasing the waist size if more optical power is available.
- Zeeman shifts: If the polarization components are known, (see comment on π component error mitigation), the systematic shifts due to the Zeeman structure can be calculated and taken into account. Furthermore, these shifts are suppressed for larger detunings.
- Influence of micromotion: This error on the 10^{-4} level will be strongly suppressed if a more suitable trap is used, where micromotion along the direction of the off-resonant beam can be fully compensated.
- Finite $D_{3/2}$ -lifetime and Residual 866 nm repump light: The finite $D_{3/2}$ -lifetime can be taken into account by incorporating it into the rate equation model. The residual optical power at 866 nm can be reduced by several orders of magnitude by using a second acousto-optical or electro-optical switch. Both effects are further suppressed for shorter depolarization times.